Overexpression of the CORVET complex alleviates the fungicidal effects of fludioxonil on the yeast *Saccharomyces cerevisiae* expressing hybrid histidine kinase 3

Received for publication, July 6, 2018, and in revised form, October 25, 2018 Published, Papers in Press, November 16, 2018, DOI 10.1074/jbc.RA118.004736

Anmoldeep Randhawa[‡1], **Debasree Kundu**[‡§2], **Anupam Sharma**[‡1], **Rajendra Prasad**[¶], **and Alok K. Mondal**[§3]

From the [‡]*Council of Scientific and Industrial Research (CSIR)-Institute of Microbial Technology, Sector 39A, Chandigarh 160036, India,* [§]*School of Life Sciences, Jawaharlal Nehru University, New Delhi 110067, India, and* [¶]*Amity Institute of Integrative Sciences and Health, Amity University, Gurgaon 122413, India*

Edited by Chris Whitfield

The hybrid histidine kinase 3 (HHK3) is a highly conserved sensor kinase in fungi that regulates the downstream HOG/p38 mitogen-activated protein kinase (MAPK). In addition to its role in osmoadaptation, HHK3 is involved in hyphal morphogenesis, conidiation, virulence, and cellular adaptation to oxidative stress. However, the molecular mechanisms by which it controls these processes remain obscure. Moreover, HHK3 is a molecular target for antifungal agents such as fludioxonil, which thereby interferes with the HOG/p38 pathway, leading to the abnormal accumulation of glycerol and subsequent cell lysis. Here, we used a chemical genomics approach with the yeast *Saccharomyces cerevisiae* to better understand the fungicidal action of fludioxonil and the role of HHK3 in fungal growth and physiology. Our results indicated that the abnormal accumulation of glycerol is not the primary cause of fludioxonil toxicity. Fludioxonil appears to impair endosomal trafficking in the fungal cells. We found that the components of class C core vacuole/endosome tethering (CORVET) complex are essential for yeast viability in the presence of a subthreshold dose of fludioxonil and that their overexpression alleviates fludioxonil toxicity. We also noted that by impeding secretory vesicle trafficking, fludioxonil inhibits hyphal growth in the opportunistic fungal pathogen *Candida albicans*. Our results suggest that HHK3 regulates fungal hyphal growth by affecting vesicle trafficking. Together, our results reveal an important role of CORVET complex in the fungicidal action of fludioxonil downstream of HHK3.

The incidence of fungal infections has been on the rise in recent decades. Fungi infect more than a billion people, causing 1.5 million deaths annually (1, 2). We have a limited armamentarium of antifungal drugs to combat this burgeoning disease burden, and the emergence of strains resistant to these drugs has aggravated this problem further (2, 3). Interestingly, the number of antifungal drugs used in agricultural practices is much larger than those used clinically. Proper understanding of the mode of action of these antifungals can provide novel insight for developing new fungicides (4). Fludioxonil is a new-generation fungicide that is widely used in agricultural practices, particularly for the postharvest management of seed and fruit preservation (5–7). Chemically, it belongs to the phenylpyrrole class of antifungal compounds and is derived from pyrrolnitrin, an antifungal secondary metabolite from *Pseudomonas pyrrocinia*. It is effective against a wide range of fungal species that belong to different genera. The mode of action of fludioxonil is quite distinct from human antifungal drugs as it targets HOG[4]/p38 MAPK signal transduction pathway (6, 7). The HOG/p38 MAPK pathway is ubiquitous in fungi and mediates cellular adaptation to high osmolarity and oxidative stress (8). In *Saccharomyces cerevisiae*, the HOG/p38 MAPK pathway is regulated by the hybrid histidine kinase Sln1p through a multistep phosphorelay involving SLN1–YPD1–SSK1. The exposure to high osmolarity causes transient activation of Hog1p by phosphorylation. The phosphorylated Hog1p enters the nucleus, resulting in transcriptional reprogramming, which is essential for the adaptation. This includes an increased synthesis and accumulation of osmolytes like glycerol to prevent the water loss (8).

Exposure to fludioxonil causes constitutive activation of the p38/HOG pathway in fungi (9). Transcriptional profiling of *Aspergillus nidulans* exposed to fludioxonil and osmotic stress also revealed that fludioxonil recapitulates the osmotic stress signal (10). Interestingly, the fungicidal effect of fludioxonil was greatly enhanced by mutation in the cell wall integrity pathway, by inhibitors of calcineurin or compounds causing oxidative stress (11). Fludioxonil treatment was shown to cause an increase in the intracellular glycerol content, hyphal swelling,

This work was supported by Department of Biotechnology, India Research Grant BT/PR5057/BRB/10/1059/2012 (to A. M. and R. P.) and Department of Science and Technology (DST), India Grant EMR/2016/001927 and DST Promotion of University Research and Scientific Excellence (PURSE) II (to A. M.). The authors declare that they have no conflicts of interest with the contents of this article.

This article contains Figs. S1–S8 and Tables S1 and S2.

[1] Recipients of a senior research fellowship from the Council of Scientific and Industrial Research, India.

[2] Recipient of a senior research fellowship from the University Grants Commission, India.

[3] To whom correspondence should be addressed. Tel.: 911126704514; E-mail: akmondal@mail.jnu.ac.in.

[4] The abbreviations used are: HOG, high-osmolarity glycerol; MAPK, mitogen-activated protein kinase; HHK, hybrid histidine kinase; CORVET, class C core vacuole/endosome tethering; SD, synthetic defined; DSP, deletion-sensitive profile; SNARE, soluble *N*-ethylmaleimide–sensitive factor (NSF) attachment protein receptor; HOPS, homotypic fusion and vacuole protein sorting; GO, gene ontology; LY, Lucifer yellow; FRAP, fluorescence recovery after photobleaching; SSRE, synthetic Skn7 response element; aa, amino acids; DAPI, 4′,6-diamidino-2-phenylindole.

and metabolite leakage in the fungal cells (6, 7). Based on these observations, it is suggested that fludioxonil interferes with the osmosensing signal transduction pathway, leading to the abnormal accumulation of glycerol and subsequent cell lysis (6, 7).

The molecular target of fludioxonil toxicity is Nik1 orthologs or hybrid histidine kinase 3 (HHK3) (6, 12–14). Initial evidence in this regard came from analyzing laboratory-generated and naturally isolated fludioxonil-resistant mutants. Both point and deletion mutations in HHK3 led to the osmosensitive and fludioxonil-resistant phenotype in many fungal species (8, 15–18). The budding yeast *S. cerevisiae* does not contain any HHK3 and is naturally not sensitive to fludioxonil. However, the heterologous expression of HHK3 confers fludioxonil sensitivity to this host, which further confirms the role of HHK3 in the toxic effect of fludioxonil on fungal cells (19–21). HHK3 is one of the most conserved and widely characterized among the fungal HHKs (14, 22). Analysis of the HHK3 mutants in several species indicates that it functions as a sensor upstream of the HOG/p38 MAPK pathway. HHK3 was found to complement Sln1p in *S. cerevisiae* and regulate the HOG/p38 MAPK pathway in a similar manner (13, 20, 22). Fungicidal action of fludioxonil involves inhibition of HHK3, resulting in the constitutive activation of the Hog1p MAPK in fungi. Similar to HHK3, the null mutation in HOG1 also showed resistance to fludioxonil (9). Apart from its role in osmoadaptation, HHK3 was also found to have a role in morphogenesis, virulence, cellular adaptation to oxidative stress, cell wall integrity, and conidiation in a number of species (14, 23–28). However, the molecular mechanism elaborating the role of HHK3 in these processes remained unknown.

In this study, we used *S. cerevisiae* and *Candida albicans* models to understand the fungicidal action of fludioxonil. *C. albicans* was included to check the effect of fludioxonil on the filamentous form of growth. Our results indicated that the abnormal accumulation of glycerol was not the primary cause of fludioxonil toxicity. Chemical genetic profiling suggested that vesicle trafficking could be one of the major processes affected by fludioxonil toxicity. The components of class C core vacuole/endosome tethering (CORVET) complex (29) were essential for viability in the presence of a subthreshold dose of fludioxonil. Fludioxonil treatment caused vacuolar fragmentation and disruption of endocytosis in yeast. Interestingly, the overexpression of some of the components of the CORVET complex, *e.g. VPS11*, *VPS16*, and *VPS18*, could abrogate the fludioxonil toxicity, therefore indicating their direct role in this process. We have shown that fludioxonil inhibits hyphal growth in *C. albicans* by impeding vesicle trafficking, and the overexpression of CaVps16 or CaVps18 could reverse this. Our data showed, for the first time, an important role of CORVET complex in the fungicidal action of fludioxonil downstream of HHK3.

Results

Fludioxonil exerts its toxic effect on S. cerevisiae expressing a heterologous HHK3 (ClNik1p) by dominantly activating the HOG/p38 pathway

ClNik1p is an HHK3 from pathogenic yeast *Candida lusitaniae* (24). In earlier studies, we have shown that *ClNIK1* could complement *sln1* deletion and act as *bona fide* osmosensor in *S. cerevisiae* (30). To create an experimentally amenable model for fludioxonil toxicity, we transformed pClNIK1 into *S. cerevisiae* strain BY4741. The cells harboring pClNIK1 became highly sensitive to fludioxonil (Fig. 1*a*). In contrast, the parental strain was resistant to the drug. The cells expressing the constitutively active mutants of ClNik1p (ΔH4 and ΔH1–4) remained resistant to fludioxonil. This observation further confirmed that the sensing competence of HHK3 was indispensable for fludioxonil toxicity. Heterologous expression of ClNik1p also conferred fludioxonil sensitivity to another *S. cerevisiae* strain, NM2, having a different genetic background (Fig. S1). One of the hallmarks of fludioxonil toxicity is the activation of the HOG/p38 MAPK pathway (6, 20–22). Therefore, we determined the phosphorylation of Hog1p by immunoblotting of the total protein extracts from the cells treated with fludioxonil. Hog1p was found to be phosphorylated within 5 min of exposure to the drug (Fig. 1, *b* and *c*), and the phosphorylated Hog1p could be detected even after 12 h (data not shown). This pattern is quite distinct from the high osmolarity–induced activation of Hog1p where the activation of Hog1p is transient and returns to the basal level mostly within 1 h (8). Earlier studies showed that DhNik1p, an HHK3 from the yeast *Debaryomyces hansenii*, regulated the HOG/p38 MAPK pathway through Ypd1p–Ssk1p phosphorelay in *S. cerevisiae* in a manner similar to that of Sln1p (13, 20, 22). ClNik1p could also be acting through Ypd1p to regulate Hog1p. To test the direct interactions between ClNik1p and *S. cerevisiae* Ypd1p, we performed a yeast two-hybrid assay. Dilution spotting on the selection plates clearly indicated that the ClNik1p (bait)/Ypd1p (prey) combination showed moderate growth. In comparison, Sln1p/Ypd1p combination showed much higher growth. The control empty prey or empty vectors showed very little or no growth (Fig. 1*d*). These results suggested that Ypd1p could interact with both ClNik1p and Sln1p. However, the interaction with the latter was much stronger. These results were further reiterated with a liquid growth assay, which showed greater than 2-fold more growth with Sln1p/Ypd1p than with ClNik1p/Ypd1p (Fig. S2). We also utilized a synthetic Skn7 response element (SSRE)-LacZ reporter system (20) to measure the histidine kinase activity of ClNik1p *in vivo*. The *S. cerevisiae* strain YSH2472 expressing ClNik1p showed a high level of β-gal activity, and the addition of fludioxonil greatly diminished this activity (Fig. 1*e*). Our results indicated that fludioxonil exerts its toxic effect by inhibiting ClNik1p and the downstream phosphorelay via Ypd1p–Ssk1p in *S. cerevisiae* even in the presence of a functional Sln1p. Both Sln1p and ClNik1p can act in parallel and independently on the downstream phosphorelay. Activation of Hog1p can only occur when both are inactivated. Thus, the inhibition of the kinase activity of ClNik1p by fludioxonil affected the downstream phosphorelay in a dominant manner by also suppressing the Ypd1p–Ssk1p phosphorelay through Sln1p.

Increased accumulation of glycerol and the nuclear translocation of Hog1p are not essential for fludioxonil toxicity

Activation of the HOG/p38 pathway causes increased synthesis and accumulation of glycerol in the cell as a part of the

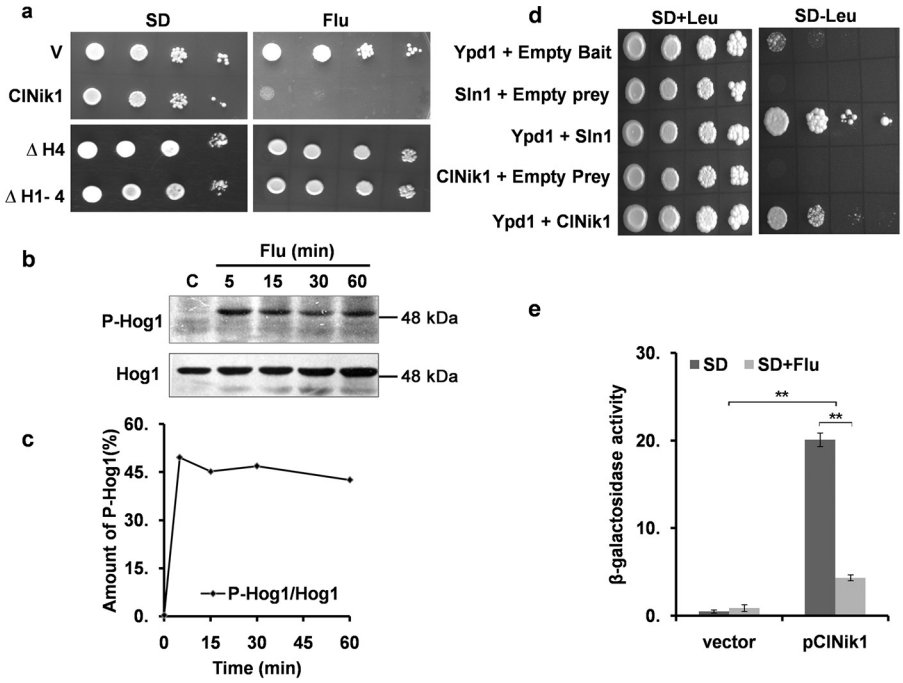

Figure 1. ClNIK1 confers fludioxonil sensitivity to *S. cerevisiae*. *a*, dilution spotting of BY4741 harboring pRS423 (*V*), pClNIK1, or its mutants. 5 μl of a 10-fold serial dilution of exponential-phase cultures grown in SD medium were spotted on an SD agar plate containing 5 μg/ml fludioxonil (*Flu*). Plates were incubated at 28 °C for 2 days. *b*, immunoblot showing fludioxonil-induced Hog1p phosphorylation in *S. cerevisiae* strain BY4741 expressing ClNik1p. Cells were grown in SD minimal medium without histidine at 28 °C to logarithmic phase and treated with fludioxonil (5 μg/ml) for different times. Total cell extract from these samples was immunoblotted using anti-phospho-p38 antibody for phospho-Hog1p (*P-Hog1*) and anti-Hog1 antibody for total Hog1p (*Hog1*). *C*, control. *c*, graph showing the time course of Hog1p phosphorylation. Values are expressed as a percentage of Hog1p as obtained by densitometric analysis of Western blotting data. *d*, two-hybrid interactions of Ypd1p with Sln1p and ClNik1p. *S. cerevisiae* strain EGY48 transformed with different bait/prey constructs was grown in minimal SD medium, and a serial dilution of the culture was spotted onto a minimal SD and galactose-raffinose plate. *e*, *in vivo* histidine kinase activity of ClNik1p in the presence of fludioxonil. β-Gal activity in the yeast strain YSH2472 harboring pClNIK1 was determined after growth in minimal liquid medium in the absence (*dark gray*) or presence of 5 μg/ml fludioxonil (*light gray*). Experiments were repeated with two independent pools of six transformants each. β-Gal activity is expressed as nmol of *o*-nitrophenyl β-galactoside utilized/min by 1 ml of culture, which was normalized to an A_{600} of 1.0. The results are presented as mean $\pm$ S.D. ($n = 9$). **, $p < 0.001$. *Error bars* represent S.D.

cellular adaptation to high-osmolarity stress (8). Because fludioxonil also activates the HOG/p38 pathway, it was hypothesized that the accumulation of glycerol causes swelling of the cell and thereby leads to various morphological defects and ultimately growth inhibition (6, 7, 11, 16). In such a scenario, the cells lacking glycerol-3-phosphate dehydrogenase, a key enzyme in the first step of glycerol biosynthesis in yeast, should be resistant to fludioxonil. This enzyme is encoded by two redundant genes, *GPD1* and *GPD2* (31). Therefore, we checked the fludioxonil sensitivity of the mutant strains Y13718 (Δ*gpd1*) and 512 (Δ*gpd1*Δ*gpd*2). The expression of ClNik1p in these mutant strains conferred sensitivity to fludioxonil that was quite similar to that of WT (Fig. 2*a*). We next compared the intracellular level of glycerol in Y13718/pClNIK1 and 512/pClNIK1 after 3 h of fludioxonil exposure. The intracellular glycerol content of Δ*gpd1* mutant was lesser than that of the parental control BY4742/pClNIK1 in the normosmolar condition. However, there was a 2-fold increase in the glycerol content in both BY4742/pClNIK1 and Y13718/pClNIK1 strains after fludioxonil treatment. In contrast, there was no increase in glycerol content in the strain lacking both *GPD1* and *GPD2* as compared with its parental control strain, which also showed a 2-fold increase in glycerol content. Thus, although Δ*gpd1*Δ*gpd2* double mutant failed to accumulate glycerol upon exposure to fludioxonil, it was sensitive to fludioxonil (Fig. 2*b*).

In response to hyperosmotic stress, Hog1p is activated and translocated to the nucleus in *S. cerevisiae*, and this is necessary for the up-regulation of several genes (including *GPD1*) required for the adaptation process. *NMD5*, a karyopherin involved in the nuclear import of proteins, plays an essential role in the nuclear translocation of Hog1p. In Δ*nmd5* cells, the stress-induced nuclear translocation of Hog1p is blocked (32). To check whether the nuclear translocation of Hog1p was essential for fludioxonil toxicity, the sensitivity of Δ*nmd5* mutant toward fludioxonil was determined. We observed that Δ*nmd5* strain expressing ClNik1p did not grow on SD (2% glucose and 0.67% yeast nitrogen base) plates containing 25 μg/ml fludioxonil; therefore, the nuclear localization of Hog1p might not be required for the antifungal activity of fludioxonil (Fig. 2*c*). To confirm this further, we monitored the subcellular localization of Hog1p-GFP. For this, *S. cerevisiae* strain BY4741 expressing ClNik1p and Hog1p-GFP were exposed to 0.4 M NaCl (osmotic shock) or fludioxonil (5 μg/ml) for 15 min. In the case of osmotic shock, 94% ($n = 138$) of cells showed strong GFP fluorescence in the nucleus. However, in the fludioxonil-treated cells ($n = 100$), the GFP fluorescence remained in the cytosol, which was quite similar to that in the untreated control samples (Fig. 2*d*). Interestingly, the cells showed similar GFP fluorescence pattern as early as 5 min and as late as 3 h of fludioxonil treatment (data not shown).

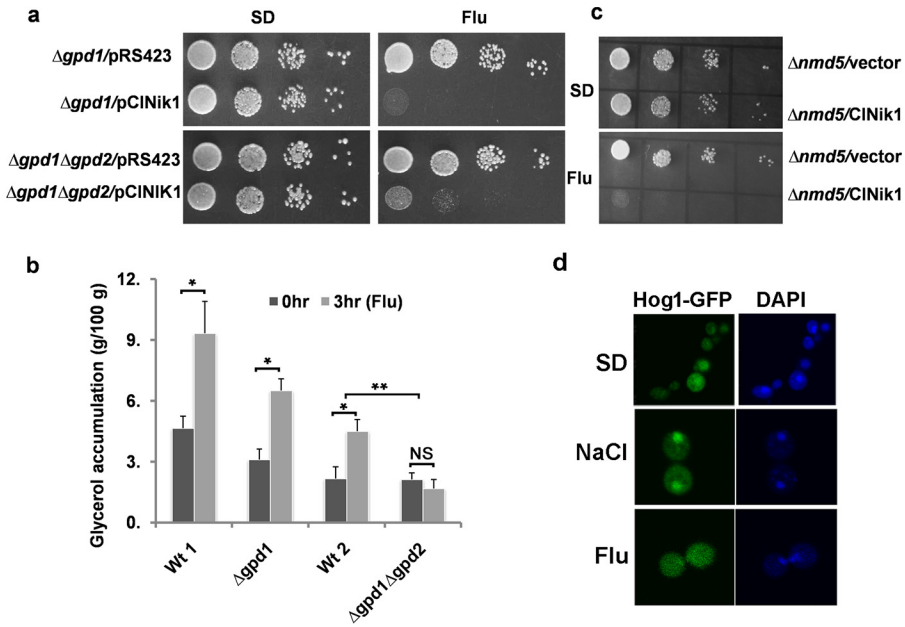

Figure 2. Role of intracellular glycerol accumulation in the antifungal activity of fludioxonil. *a*, dilution spotting of *S. cerevisiae* strains Y13718 (Δ*gpd1*) and 512 (Δ*gpd1*Δ*gpd2*) harboring vector pRS423 or pCINIK1 on an SD agar plate with or without 25 μg/ml fludioxonil (*Flu*). *b*, intracellular glycerol content of *S. cerevisiae* strains BY4742 (*Wt 1*), Y13718, 507 (*Wt 2*), and 512 harboring pClNIK1. Cultures at mid-exponential phase were exposed to 25 μg/ml fludioxonil for 3 h, and the amount of glycerol in total cell extract was measured using a UV glycerol assay kit (R-Biopharm) and normalized to dry weight of the cell. Results of two independent experiments performed in duplicates are presented as mean ± S.D. ($n = 4$). *NS*, not significant; *, $p < 0.01$; and **, $p < 0.001$. *Error bars* represent S.D. *c*, dilution spotting of *S. cerevisiae* strains B0119B (Δ*nmd5*) harboring p426TEF (vector) or p426TEF-CINIK1 (ClNik1) on an SD agar plate with or without 25 μg/ml fludioxonil. *d*, cellular localization of Hog1-GFP. Log-phase cultures of BY4741 harboring plasmids pClNIK1 and pHog1-GFP were treated with 0.4 M NaCl or 5 μg/ml fludioxonil for 15 min. After fixing cells with paraformaldehyde and staining with DAPI, GFP fluorescence in the untreated (SD) and treated samples was observed under a fluorescence confocal microscope.

A genome-wide phenotypic screen identified yeast deletion strains hypersensitive to fludioxonil

Glycerol accumulation was not the primary cause of fludioxonil toxicity. In an attempt to identify the primary cause of the cytotoxicity, we systematically screened the haploid deletion strain collection of *S. cerevisiae* (33, 34). Each deletion strain (BY4741 genetic background) was individually transformed with plasmid pClNIK1 using a high-throughput 96-well plate transformation protocol (35). The relative growth assays of the transformants were performed in the presence of 0.76 μg/ml fludioxonil in a 96-well format. Strains having less than 60% growth compared with the WT control were shortlisted as hypersensitive strains. In the preliminary screening, among the ~5000 deletion strains, 290 strains were found to be hypersensitive to fludioxonil. To weed out the false positives, the sensitive strains identified in the initial screening were separated from the rest of the library into four 96-well plates and transformed again with pClNIK1. The growth of the transformants was measured at two concentrations of fludioxonil, *i.e.* at 0.75 and 0.5 μg/ml. Two different doses were used to increase the stringency of the screening. Finally, only those strains that showed consistent hypersensitivity and a *z* value below 0 at both concentrations were selected (Fig. S3). Five strains showing consistent hypersensitivity only at 0.75 μg/ml fludioxonil were included in the list. Any strain sensitive to 0.5 μg/ml fludioxonil should theoretically also be sensitive to the higher concentration of the drug. Therefore, six strains that were found only in the data set with 0.5 μg/ml fludioxonil were considered false positives and ignored (Fig. S3). Furthermore, 21 strains showing a slow growth phenotype and eight dubious ORFs were also ignored. Previously, Parsons *et al.* (36) carried out chemical genetic profiling of 82 bioactive compounds and identified a set of 121 deletion mutants that displayed statistically significant sensitivity to these compounds (multidrug-sensitive profile). Nine strains from the multidrug-sensitive profile were found to be present in the deletion-sensitive profile (DSP) of fludioxonil and thus were also excluded from the concluding list (Fig. S3). Finally, the DSP of fludioxonil identified 60 genes (Table S1) whose deletion caused hypersensitivity to fludioxonil. Δ*bck1*, Δ*slt2*, Δ*hof1*, Δ*mit1*, and Δ*vam7* were the most hypersensitive to fludioxonil among these 60 strains. Bck1p and Slt2p are integral to the cell wall integrity pathway (37). Hof1p plays an important role in cytokinesis (38, 39). Vam7p is an important vacuolar SNARE involved in vacuole fusion (40), and Mit1p is a transcriptional regulator of pseudohyphal growth in *S. cerevisiae* (41).

To identify the pathways affected among 60 hypersensitive strains, the online data mining tool DAVID (42) was used. A comprehensive analysis by DAVID revealed that ~30% of the genes in the DSP of fludioxonil were involved in the establishment of localization of proteins, and more than 6% of the genes were found to be involved in cytokinesis and vacuole fusion. Overrepresented gene ontologies belonged to five major cell processes, *e.g.* protein targeting (establishment of protein localization and endoplasmic reticulum unfolded protein response), vacuole organization (vacuole fusion and HOPS and CORVET complexes), cell wall integrity pathway (cell wall glycoprotein biosynthetic process and cell wall biogenesis), cytokinesis (barrier septum formation and mannosyltransferases), and transcriptional machinery (chromatin remodeling complex and

Srb-mediator complex). Analysis using gene ontology (GO) term Slim Mapper revealed that the GO terms "endosomal transport" and "vacuole organization" were 6- and 5-fold enriched in our DSP gene list, respectively, as compared with total gene space (Fig. 3*b*). More than 2-fold enrichment of GO terms *e.g.* vesicle organization, membrane fusion, endocytosis, and cytokinesis was also observed in this list. The analysis of the network of interaction forms by the genes of our DSP set by GeneMANIA (43) also highlighted the roles endosomal transport and vesicle fusion (Fig. 3*c*). The CORVET complex appeared to be the most prominent protein complex with a role in fludioxonil toxicity. To rule out the possibility of the phenotype arising due to the accumulation of any additional mutation(s) in the deletion strains of the library, we recreated deletion mutations of CORVET subunits (*VPS3*, *VPS8*, *VPS11*, *VPS16*, and *VPS18*), SNARE proteins (*VAM6* and *VAM7*), and *VPS9* in the BY4741 background and reconfirmed the fludioxonil hypersensitivity of these mutants (Fig. S4).

Fludioxonil impairs cytokinesis in S. cerevisiae model

Δ*hof1* was identified as one of the most fludioxonil-hypersensitive strains. Hof1p is a F-Bar (having a SH3 domain) protein involved in cytokinesis in yeast, and it directly regulates formin activity and secretory vesicle trafficking during polarized cell growth (39). Hof1p localizes at the bud neck as soon as the new cell cycle is commenced. It colocalizes with the septin ring until late anaphase and then shifts to the actomyosin ring just before ring contraction (38). We examined the effect of fludioxonil on the localization of Hof1p-GFP in *S. cerevisiae*. For this, the BY4741 strain having chromosomal GFP-tagged Hof1p was transformed with pClNIK1 plasmid. The transformants were grown in SD medium (−His,−Ura) to an A_{600} of 0.5–0.7. An aliquot of the culture was centrifuged, and cells were fixed in 4% paraformaldehyde for 10 min to serve as a control. The rest of the culture was treated with fludioxonil (25 μg/ml) for 3 h and processed similarly. In more than 60% of the budded cells in the control sample, Hof1p was found to be localized on the bud neck. However, in the fludioxonil-treated cells, less than 20% of the budded cells had Hof1p-GFP localized on the bud neck (Fig. 4, *a* and *b*). This result suggests that fludioxonil impedes the localization of the proteins at the bud neck, which is essential for cytokinesis.

We next examined the effect of fludioxonil on the cell cycle and budding pattern in our *S. cerevisiae* model. For this, yeast strain BY4741/ClNik1p was synchronized using α-factor. 58% of the cells resumed growth in SD medium within 30 min after the release from α-factor arrest. However, upon exposure to fludioxonil, the cells showed a delayed exit from G_1 phase as 86% of cells were nonbudded even after 1 h of release from α-factor arrest. We analyzed the nuclear division pattern of the budded cells in the control and treated samples (Fig. 4*c*). It was observed that 63% of the budded cells had a single nucleus, and 37% had two nuclei in the control sample. However, after 4 h of incubation with fludioxonil, 53% of the budded cells were found to have two nuclei. Interestingly, 10% population of the budded cells had more than one bud and three nuclei per cell in the treated sample, and this increased to 27% after 8 h of fludioxonil treatment (Fig. 4*c*). Thus, it was speculated that fludioxonil might be inducing a cytokinesis defect, resulting in cells with multiple nuclei. To further confirm this, flow cytometry was conducted. Cells of WT strain BY4742/ClNIk1p at logarithmic phase were exposed to fludioxonil for 4 h. Cells were fixed with 70% ethanol, and flow cytometric analysis of DNA contents was carried out. The untreated control sample showed normal distribution of G_1 (29%), S (35%), and G_2 (28%) phase cells at 0 h; however, after 4 h of fludioxonil treatment, there was a remarkable decrease in the number of cells at G_1 (14%) phase and a simultaneous increase in the cell showing polyploidy (47%). These results indicated that normal cytokinesis was affected in the cells treated with fludioxonil (Fig. 4*d*).

Fludioxonil affects vacuolar morphology and impairs endocytosis

The DSP of fludioxonil was highly enriched with genes involved in the fusion of the endosome and vacuole, particularly the components of CORVET complex (29), SNARE proteins, and their regulators (40). Endosomes receive cargo from various pathways and constantly undergo fission and fusion events. Fusion of early endosomes is regulated by the CORVET complex, whereas late endosome/vacuole fusion is regulated by its sibling, the HOPS complex. Both are hexaheteromeric complexes with common subunits, *VPS11*, *VPS16*, *VPS18*, and *VPS33*. To examine the effect of fludioxonil on late endosome fusion, we monitored vacuolar morphology using the fluorescent dye FM4-64 (Fig. 5*a*). In the control samples, 67.5% of the cells ($n = 425$) showed a single large vacuole, and only 2.8% cells showed highly fragmented vacuoles. In contrast, only 5.57% of the yeast cells ($n = 341$) had a single large vacuole in the fludioxonil-treated sample. The majority of the cells (90.9%) were found to have fragmented vacuoles. Vacuoles were found to be fragmented within 2 min of fludioxonil treatment and to remain fragmented even after 3 h of treatment. Thus, fludioxonil toxicity inhibited the fusion of the vacuole in *S. cerevisiae* expressing ClNik1p. In *S. cerevisiae*, the CORVET complex is found on endosomal dots (44). We therefore monitored the effect of fludioxonil on CORVET localization of Vps8-GFP fusion protein. Vps8 is a subunit specific to the CORVET complex. In control cells, Vps8-GFP was visible in two to three bright endosomal dots (Fig. 5*b*). In the fludioxonil-treated cells, GFP fluorescence was largely diffused. Some cellular dots with much lower fluorescence intensity remained nevertheless (Fig. 5*b*). This result indicated cytosolic localization of CORVET subunit Vps8. To confirm this further, the total cell lysate was subjected to subcellular fractionation by high-speed centrifugation (100,000 × *g*). The P100 fraction, which was enriched in Golgi membranes and small vesicles, including endosomes, and the S100 fraction, which contained cytosolic molecules, were immunoblotted with anti-GFP antibody (SC 8334, Santa Cruz Biotechnology) to detect Vps8-GFP fusion protein. In the control untreated sample, Vps8-GFP was detected only in the P100 fraction, whereas in the fludioxonil-treated samples a significant amount of Vps8 was also present in the S100 fraction (Fig. 5*c*). Taken together, these results clearly demonstrated that fludioxonil impedes endosomal trafficking by interfering with CORVET localization.

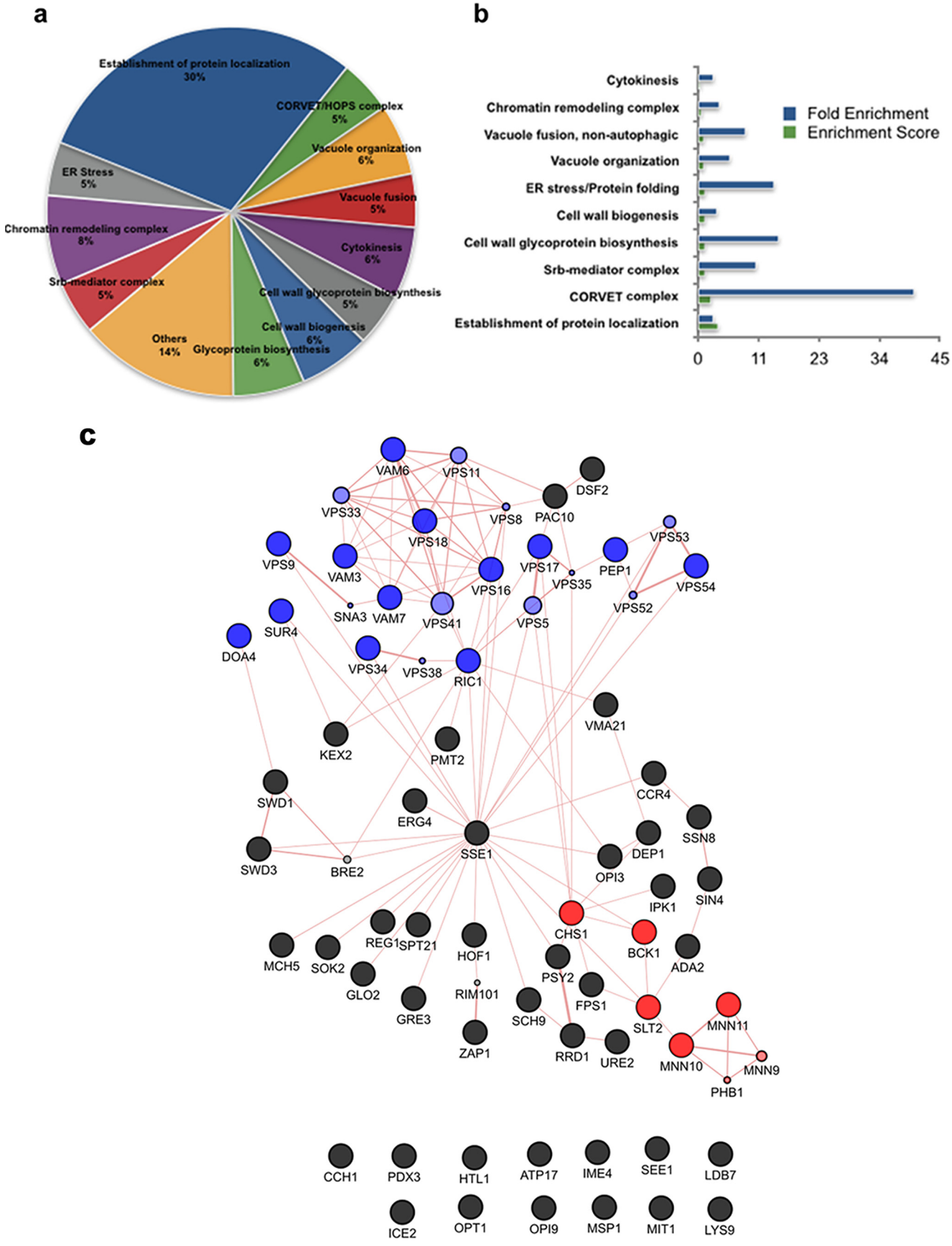
a
Establishment of protein localization 30%
CORVET/HOPS complex 5%
Vacuole organization 6%
Vacuole fusion 5%
Cytokinesis 6%
Cell wall glycoprotein biosynthesis 5%
Cell wall biogenesis 6%
Glycoprotein biosynthesis 6%
Others 14%
Srb-mediator complex 5%
Chromatin remodeling complex 8%
ER Stress 5%
b
Cytokinesis
Chromatin remodeling complex
Vacuole fusion, non-autophagic
Vacuole organization
ER stress/Protein folding
Cell wall biogenesis
Cell wall glycoprotein biosynthesis
Srb-mediator complex
CORVET complex
Establishment of protein localization
Fold Enrichment
Enrichment Score
0
11
23
34
45
c
VAM6
VPS11
DSF2
VPS33
VPS8
PAC10
VPS18
VPS53
VPS9
VAM3
VPS17
PEP1
VPS16
VPS35
VPS54
SNA3
VAM7
VPS41
VPS5
VPS52
SUR4
DOA4
VPS34
VPS38
RIC1
VMA21
KEX2
PMT2
SWD1
CCR4
ERG4
SSN8
SSE1
DEP1
SWD3
BRE2
OPI3
IPK1
SIN4
CHS1
REG1
SPT21
HOF1
BCK1
MCH5
SOK2
PSY2
ADA2
GLO2
RIM101
FPS1
GRE3
SCH9
SLT2
MNN11
ZAP1
RRD1
URE2
MNN10
MNN9
PHB1
CCH1
PDX3
HTL1
ATP17
IME4
SEE1
LDB7
ICE2
OPT1
OPI9
MSP1
MIT1
LYS9

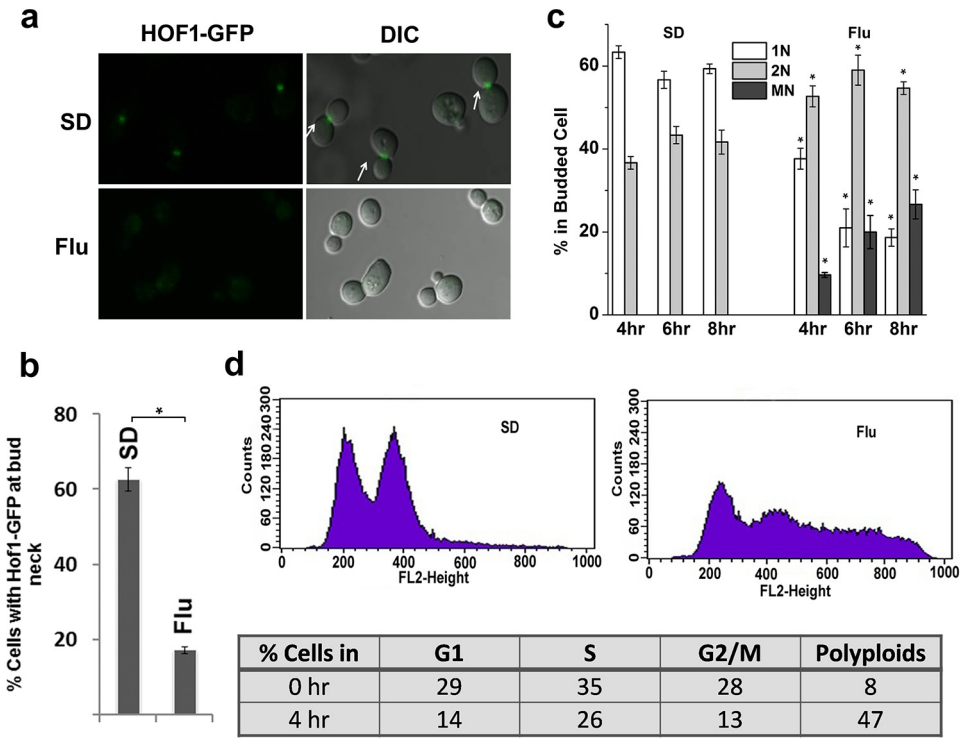

% Cells in	G1	S	G2/M	Polyploids
0 hr	29	35	28	8
4 hr	14	26	13	47

Figure 4. Effect of fludioxonil on the cell cycle. *a*, localization of Hof1-GFP in BY4741/pClNIK1. Cells at logarithmic phase were treated with fludioxonil (*Flu*) (25 μg/ml) for 3 h and observed under a microscope after fixing with paraformaldehyde. Localization of Hof1-GFP at the bud neck in the control untreated cells is shown by an *arrow*. *DIC*, differential interference contrast. *b*, graph showing the percentage of budded cells having Hof1-GFP localized at the bud neck. More than 100 cells were counted for each sample, and the data (mean ± S.D.) presented are from three independent experiments. *, $p < 0.05$. *Error bars* represent S.D. *c*, an early log-phase culture of BY4741/pClNIK1 synchronized by α-factor was released into fresh SD medium with or without 25 μg/ml fludioxonil. Cells were harvested at different times, stained with DAPI to monitor nuclear division, and observed under a microscope as described under "Experimental procedures." The number of nuclei was counted in more than 100 budded cells in each sample (*1N*, *2N*, and *MN* represent one, two, and three nuclei per cell). Results of three independent experiments are presented as mean ± S.D. *, $p < 0.05$. *Error bars* represent S.D. *d*, DNA content of *S. cerevisiae* strain BY4742/pClNIK1 with or without fludioxonil treatment was determined by flow cytometry as described under "Experimental procedures." The *x axis* represents relative DNA content. The *left-most* peak represents the G_1 population, and the *right-most* peak represents the G_2 population. Representative data from three independent experiments are shown.

To check the effect of fludioxonil on vesicle trafficking further, we carried out Lucifer yellow (LY) uptake assay (45). LY enters the cells through fluid-phase endocytosis and accumulates in the vacuole, which depends on the endocytic transport route, passing through intracellular endosomal compartments. BY4741/pClNIK1 cells at logarithmic phase with or without fludioxonil treatment were incubated with LY for 45 min. In the control samples, vacuoles were prominently stained with LY, whereas in the fludioxonil-treated cells very little or no LY stain was visible (Fig. 5*d*). We also conducted an FM4-64 recycling assay (45). For this, BY4741/pClNIK1 cells at logarithmic phase were treated with fludioxonil and allowed to take up FM4-64 for 12 min. After thorough washing with ice-cold SD medium, the cells were resuspended in warm medium, and fluorescence associated with the cells was measured. In the control untreated sample, the fluorescence was decreased to ~40% within 20 min. However, the fludioxonil-treated cells could retain ~80% of the fluorescence at this time point (Fig. 5*e*). These results clearly indicated that vesicle trafficking was compromised in fludioxonil-treated cells.

Overexpression of the components of CORVET complex abrogates fludioxonil toxicity

Previous studies indicated that the genes that confer hypersensitivity when deleted could be directly related to the drug's mechanism of action if they also exhibit resistance when overexpressed (34). We therefore, investigated whether the overexpression of the identified genes could confer resistance to fludioxonil. For this, we expressed *VPS8*, *VPS9*, *VPS11*, *VPS16*, *VPS18*, *VAM3*, *VAM6*, *VAM7*, *VPS34*, *VMA21*, *BCK1*, and *SLT2* from the high-copy-number plasmid pRS426 in BY4741/pClNIK1 and determined fludioxonil sensitivity of these strains by dilution spotting. *BCK1*, *SLT2*, *VPS34*, and *VMA21* were included in our analysis as internal controls. *BCK1* and *SLT2* are members of the cell wall integrity pathway and were present in the most hypersensitive list, whereas *VSP34* and *VMA21* are important regulators of vacuole function but do not belong to the tethering complex. Fludioxonil sensitivity of the strains expressing *VPS8*, *VAM3*, *VPS34*, *VMA21*, *BCK1*, and *SLT2* was quite similar to that of the host. *VPS9*, *VAM6*, and *VAM7* con-

Figure 3. GO enrichment of deletion strains hypersensitive to fludioxonil. *a*, pie chart describing the number and distribution of enriched GO terms obtained from DAVID analysis of fludioxonil deletion-sensitive profile. *b*, enrichment score and -fold enrichment of the identified GO terms. *c*, interaction network generated by GeneMANIA. *Edges* indicate physical interactions between gene products; *edge weights* reflect confidence in support for interactions. *Blue* node color corresponds to a set of functional gene classes involved in endosomal transport and vesicle fusion. Genes involved in cell wall biosynthesis are shown in *red*. *Light-colored* nodes were not part of the input set.

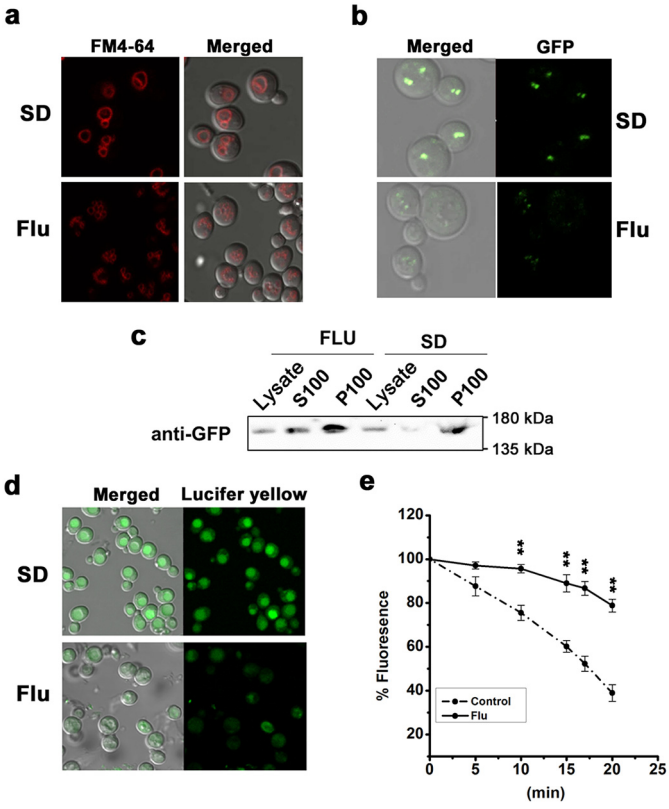

Figure 5. Effect of fludioxonil on vacuolar morphology and vesicle trafficking. *a*, *S. cerevisiae* strain BY4741/pCINIK1 was treated with 5 μg/ml fludioxonil (*Flu*) and stained with membrane dye FM4−64 as described under "Experimental procedures." Micrographs were taken using a Nikon A1R confocal microscope. *b*, *S. cerevisiae* strain BY4741 with chromosomally tagged VPS8-GFP and harboring plasmid pCINIK1 was grown to log phase and treated with fludioxonil (5 μg/ml) for 2 h. Cells were washed with PBS and observed under a Nikon A1R confocal microscope. *c*, subcellular localization of GFP-tagged Vps8 was monitored in cells expressing CINik1 after treating with fludioxonil (5 μg/ml) for 4 h. Total cell extract (*Lysate*) were fractionated to obtain a pellet (P100) and supernatant (S100) after the final centrifugation at 100,000 $\times$ *g*. Western blots were decorated against the GFP tag to identify Vps8. *d*, effect of fludioxonil on the accumulation of LY. *S. cerevisiae* strain BY4741/pCINIK1 with or without fludioxonil treatment was incubated at 30 °C with YPD containing LY (4 mg/ml) for 45 min before being photographed using a Nikon A1R confocal microscope. *e*, real-time FM4-64 recycling assay with *S. cerevisiae* strain BY4741/pCINIK1 treated with or without fludioxonil. FM4-64 fluorescence in the cell suspension was measured for 20 min continuously in a spectrofluorometer. Results are presented as mean $\pm$ S.D. ($n = 6$). **, $p < 0.001$. *Error bars* represent S.D.

ferred a low level of resistance, whereas the cells expressing *VPS11*, *VPS16*, and *VPS18* were highly resistant to fludioxonil (Fig. 6*a*). The resistance exhibited by these cells was not caused by suppression of Hog1 activation as phosphorylated Hog1 could be detected in these cells after fludioxonil treatment (Fig. 6*b*). The examination of FM4-64–stained cells by microscopy also showed that the overexpression of *VPS11*, *VPS16*, and *VPS18* could suppress the vacuole fragmentation caused by fludioxonil toxicity (Fig. 6*d*). In the control BY4741 cells treated with fludioxonil, 84.9% of cells showed highly fragmented vacuoles. In the case of *VPS11*-, *VPS16*-, and *VPS18*-overexpressing cells, highly fragmented vacuoles were observed in 4.78, 23.63, and 45.66% cells, respectively. A significant percentage of the cells had less than three vacuoles. In comparison, the vacuole fragmentation pattern in the cells expressing all other genes was quite similar to the WT control (Fig. S5). We also observed that the pattern of Vps8-GFP localization in the cells overexpressing *VPS11*, *VPS16*, and *VPS18* was quite similar in fludioxonil-treated and untreated cells (Fig. 6*c*). Therefore, the overexpression of *VPS11*, *VPS16*, and *VPS18* could restore CORVET localization on endosomal dots in fludioxonil-treated cells. Together, these results indicated that the components of the CORVET complex could be important effectors of fludioxonil toxicity downstream of HHK3.

The fungal hypha is an example of an extreme form of polarized growth in which vesicle trafficking plays a crucial role (46). Mutants deficient in the biogenesis and fusion of secretory vesicles, early endosomes, and vacuoles have profound defects in invasive hyphal growth, conidiation, and virulence in fungi (46–48). The deletion of *CaVPS11* gene, which encodes a protein of the CORVET complex, has a severe effect on the hyphal growth and virulence in the opportunistic fungal pathogen *C. albicans* (49). We therefore assessed the effect of fludioxonil on hyphal growth in *C. albicans*. *C. albicans* can grow as single-cell yeast or filamentous hyphal form in response to diverse environmental cues. On a YPD (1% yeast extract, 2% peptone, and 2% dextrose) agar plate, *C. albicans* grew as a yeast form that was not affected by the presence of fludioxonil. However, on Spider medium or in the presence of serum, which induces filamentous growth, fludioxonil severely affected hypha formation (Fig. 7*a*). In *C. albicans*, CaTup1 is a negative regulator of hyphal growth induction, and therefore *Catup1*Δ mutant shows the filamentous form of growth constitutively (50). Fludioxonil also inhibited true hypha formation in *Catup1*Δ mutant, and the morphology of the fludioxonil-treated cells was more like a pseudohypha (Fig. S6). To corroborate this further, we determined the effect of fludioxonil on the localization of CaSpa2, which is an essential component of the polarisome complex present in the tip of the growing hypha in *C. albicans*. *C. albicans* strain WYZ9 (51) expresses CaSpa2-GFP fusion protein and harbors the *Catup1*Δ deletion mutation. In this strain, CaSpa2-GFP persistently localized on the hyphal tip (Fig. 7*b*). In the cells treated with fludioxonil, CaSpa2-GFP was nearly absent from the tip. In some cells, it prominently localized to the septa (Fig. 7*b*), and thus even in a genetic background that favors hypha formation, the polarisome protein CaSpa2p was completely mislocalized by fludioxonil treatment. During the continuous polarized growth of *C. albicans* hyphae, the vesicle-associated Rab GTPase CaSec4 localizes dynamically at the tip, corresponding to a vesicle-rich region (52). To determine the effect of fludioxonil on the localization of CaSec4-GFP on the hyphal tip, we performed a fluorescence recovery after photobleaching (FRAP) experiment (Fig. 7*d* and Fig. S7). In the control sample, the recovery of CaSec4-GFP was observed at 12–15 s postbleach. However, the recovery of CaSec4-GPF in the fludioxonil-treated hyphae was much less even 60 s postbleach. These data suggest that fludioxonil inhibits the filamentous growth in *C. albicans* by affecting vesicle trafficking.

Next, we investigated the effect of overexpression of *CaVPS16* and *CaVPS18* on fludioxonil toxicity in *C. albicans*. For this, we cloned the ORF encoding *CaVPS16* and *CaVPS18* in the plasmid vector pVT50. The resultant plasmids (pCaVPS16 and pCaVPS18) were linearized with StuI and transformed into

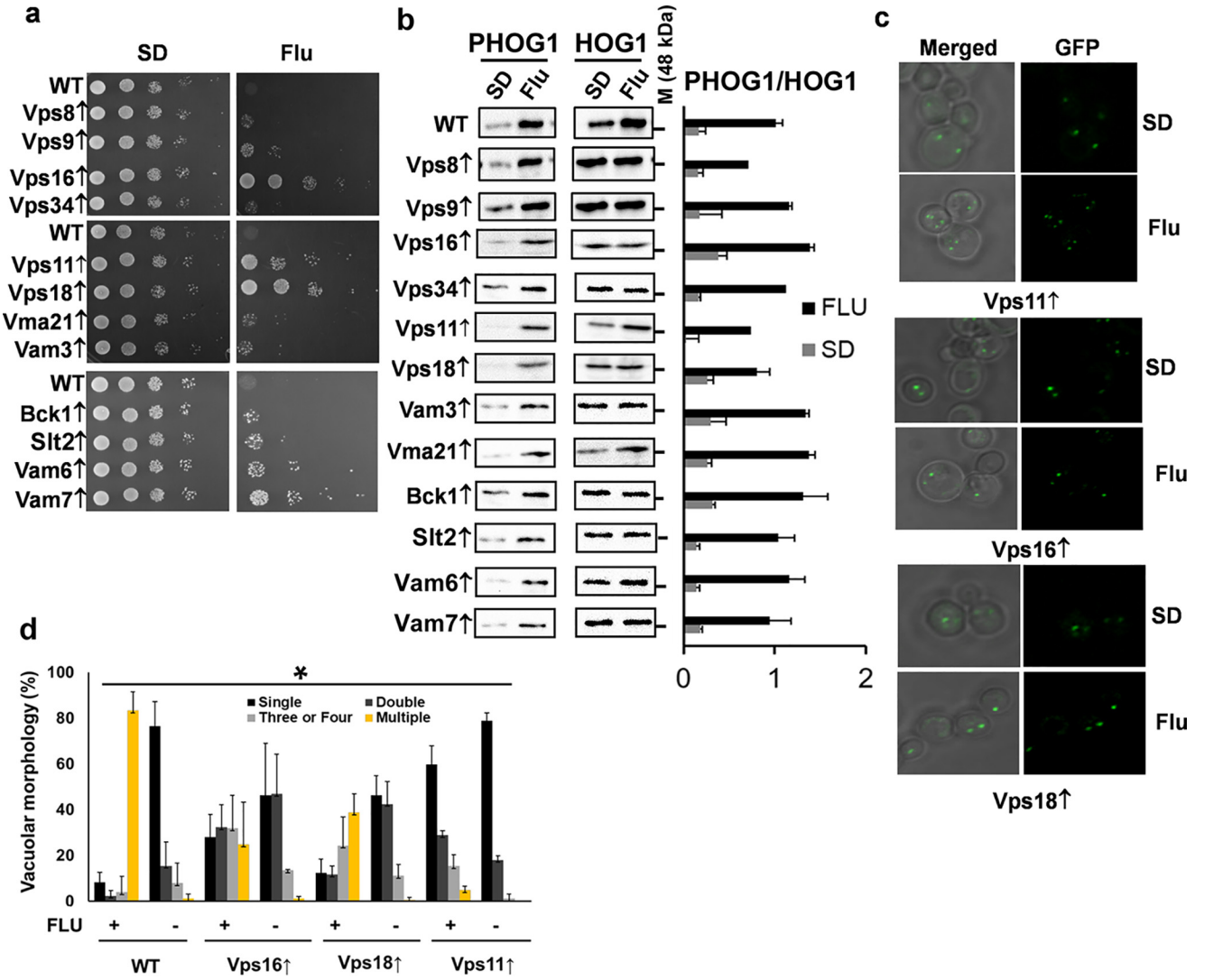

Figure 6. Overexpression of the component of CORVET complex suppresses antifungal activity of fludioxonil. *a*, dilution spotting of *S. cerevisiae* strain BY4741 harboring different genes in multicopy plasmid pRS426 along with pCINIK1 on SD or an SD agar plate with fludioxonil (*Flu*) (25 μg/ml). *b*, immunoblot showing fludioxonil-induced Hog1p phosphorylation in *S. cerevisiae* strain BY4741 harboring different genes in multicopy plasmid pRS426 along with pCINIK1. The *right panel* shows the quantification of the phosphorylated Hog1p (*PHOG1*) in the immunoblot. The values were determined by densitometry and expressed as ratio of signals, PHOG1/HOG1, of the respective lanes. Graphs are plotted as mean ± S.D. calculated from three independent blots. *Error bars* represent S.D. *c*, localization of VPS8-GFP in *S. cerevisiae* strain BY4741/pCINIK1 overexpressing Vps11, Vps16, or Vps18. Cells at logarithmic phase were treated with fludioxonil (5 μg/ml) for 2 h. Cells were washed with PBS and observed under a Nikon A1R confocal microscope. A representative figure from three independent experiments is shown. *d*, vacuole fragmentation in *S. cerevisiae* strain BY4741/pCINIK1 overexpressing Vps11, Vps16, or Vps18. Cells at logarithmic phase untreated or treated with 5 μg/ml fludioxonil were visualized after staining with the dye FM4-64. Vacuoles with different morphology were counted and expressed as a percentage (mean ± S.D.) from three independent experiments (two-way analysis of variance; *, $p < 0.05$). *Error bars* represent S.D.

C. albicans strain SC5314. Integration of the plasmid into the host genome resulted in a *C. albicans* strain expressing CaVps16 and CaVps18 from the *CaACT1* promoter. The overexpression of CaVps16 and CaVps18 in the respective clones was confirmed by RT-PCR (Fig. S8). To determine the effect of fludioxonil, these clones were grown in YPD at 30 °C up to logarithmic phase. The cells were then transferred to Spider medium with or without fludioxonil (25 μg/ml) and observed under a microscope after 4 h of incubation. In the presence of fludioxonil, the parental control strain failed to exhibit the filamentous form of growth and remained as yeast. In contrast, the filamentous form was quite evident in the clones overexpressing CaVps16 and CaVps18 (Fig. 7*e*). Thus, like that in the *S. cerevisiae* host, the overexpression of the components of CORVET complex could suppress fludioxonil toxicity in *C. albicans* as well.

Discussion

Fludioxonil is an interesting fungicide that has been used in agricultural practices for the past 30 years with nearly no incidence of developing field resistance against it (7). In this respect, fludioxonil is different from the antifungal agents used against human pathogens. Therefore, a detailed understanding of the fungicidal action of fludioxonil could pave the way to identify novel targets as well as therapeutic agent(s). Fludioxonil is known to affect the signal transduction pathway by targeting HHK3. However, the molecular events downstream of HHK3 that lead to cell death have remained obscure. To illu-

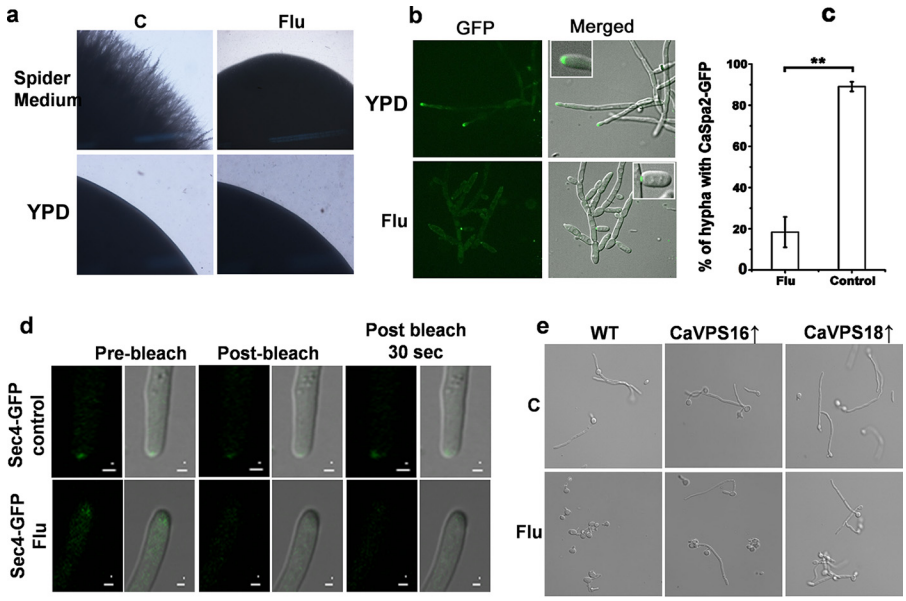

Figure 7. Fludioxonil inhibit hyphal growth in *C. albicans*. *a*, overnight cultures of *C. albicans* strain SC5314 were spotted onto YPD and a Spider agar plate with or without fludioxonil (*Flu*) (25 μg/ml) and incubated at 37 °C for 5 days. Images of colony edges were obtained using a stereomicroscope. *C*, control. *b*, fludioxonil affects the localization of CaSpa2p-GFP to the tips of filaments. Strain WYZ9 (*Catup1*Δ) expressing CaSpa2p-GFP was grown in YPD medium with or without 50 μg/ml fludioxonil at 37 °C for 6 h. Cells were washed with 1× PBS before visualizing under a microscope. *c*, percentage of hypha with CaSpa2p-GFP at the tip. The results are presented as mean ± S.D. ($n = 3$). **, $p < 0.01$. *Error bars* represent S.D. *d*, fluorescence recovery of CaSec4-GFP. *C. albicans* strain expressing CaSec4-GFP was grown in Spider medium at 37 °C for 45 min. After addition of fludioxonil (50 μg/ml), the culture was incubated further for 45 min. Cells were then embedded in 0.4% agar on glass slides for FRAP. A minimum of 10 hyphal tips of each strain were bleached, and images were recorded before bleaching (prebleach) for 30 s, 30 s after bleaching (postbleach), and 60s after bleaching. Representative images of individual hyphal tips at prebleach, postbleach, and 30 s postbleach are shown. *Bars*, 1 μm. *e*, hyphal morphology of *C. albicans* strains overexpressing CaVPS16 and CaVPS18. ORFs encoding CaVPS16 and CaVPS18 were cloned in plasmid pVT50 under the *ACT1* promoter, and the linearized plasmids were chromosomally integrated into *C. albicans* strain SC5314 at the *RP10* (ribosomal protein 10) gene locus. Cells were grown in Spider medium for 3 h at 37 °C with and without fludioxonil (25 μg/ml) and observed under a microscope. *C. albicans* strain SC5314 was used as a control (WT).

minate these processes, we used an *S. cerevisiae* model. Fludioxonil inhibited the growth of *S. cerevisiae* cells expressing ClNik1p. Interestingly, the inhibition of the activity of ClNik1p by fludioxonil dominantly affected the phosphorelay through another nontarget histidine kinase, Sln1p, although Sln1p exhibited much stronger interaction with Ypd1p (Fig. 1*d* and Fig. S2). In the presence of fludioxonil, ClNik1p could possibly be converted into a phosphatase and thereby dominantly inhibit the downstream phosphorelay. A similar mechanism has been proposed for another fungal HHK3, Drk1, recently (53). Many prokaryotic two-component histidine kinases are bifunctional as they can act as both a kinase and a phosphatase for their cognate response regulators (54). The ratio of kinase to phosphatase activity determines the output response. Although filamentous fungi have a large repertoire of HHKs, the number of response regulators and phosphotransfer proteins that act downstream of these HHKs are limited. Most species contain only two to three response regulators (55). Therefore, HHK3 can potentially regulate more than one signaling pathway by acting as a kinase or phosphatase.

Earlier studies indicated that the p38/HOG MAPK pathway plays a pivotal role in the fungicidal action of fludioxonil (14, 20, 22). Besides this pathway, involvement of the cell wall integrity pathway and calcineurin-mediated signaling have also been implicated (11). Both *MPK1* and calcineurin deletion conferred hypersensitivity to fludioxonil. Constitutive activation of Hog1p was observed in several fungal species upon fludioxonil treatment. In *Neurospora crassa* and *Cochliobolus heterostrophus* mycelia, it caused abnormal accumulation of glycerol and hyphal swelling (6). Abnormal accumulation of glycerol was also observed in other fungal species. Based on these observations, glycerol accumulation was accepted to be the primary cause of fludioxonil-mediated cell death (6, 7). In response to osmostress, fungal cells accumulate glycerol by transcriptional up-regulation of *GPD1*, which is facilitated by nuclear entry of Hog1p. To decipher the role of glycerol accumulation, we utilized a mutant (Δ*nmd1*) defective in nuclear entry of Hog1p and a mutant (Δ*gpd1*Δ*gpd2*) deficient in glycerol biosynthesis (Fig. 2). Our results clearly indicate that the cytotoxicity of fludioxonil is not solely due to the accumulation of glycerol. Some other process is also affected, and it could be the main reason for growth arrest and cell death in fungi by fludioxonil.

To decipher the primary target, we conducted a genome-wide screen and identified that the genes involved in early and late endosomal transport, *e.g.* CORVET complex and its regulators, SNARE proteins, could be potential downstream effectors of fludioxonil toxicity. The adverse effect of fludioxonil on endosomal biogenesis and vacuolar morphology was quite evident as we observed highly fragmented vacuoles after drug treatment. Fludioxonil also impaired CORVET localization on endosomal dots, indicating its effect on endosomal trafficking (Fig. 5, *b* and *c*). The LY uptake assay and FM4-64 recycling assay confirmed this further (Fig. 5, *d* and *e*). The overexpression of *VPS11*, *VPS16*, and *VPS18* conferred resistance to fludioxonil, indicating their role in the cytotoxic effect of this compound. Vps11p, Vps16p, and Vps18p are the core subunits of CORVET and HOPS tethering complexes. CORVET acts on early endosomes having Vps21/Rab5-positive membranes,

whereas HOPS mediates the fusion of late endosomal Rab7-positive membranes (29). Vps21/Rab5-positive endosomes also play a key role in vesicle trafficking during cytokinesis (56). Impairment of cytokinesis was also observed after fludioxonil treatment that could be due to the polarization defect or disrupted endosomal trafficking. CORVET and HOPS complexes interact with other endosomal maturation machinery such as phosphoinositides, endosomal sorting complexes required for transport (ESCRT) machinery, vacuolar-type (V) ATPase, actin, and microtubules (57). Thus, the effect of fludioxonil on endosomal trafficking can be an outcome of the disruption of this cooperative network. Endosomes are a central compartment in the endocytic pathway, and therefore any adverse effect on them can affect the collective vesicle trafficking capacity of the cell by interfering with recycling endosomes or protein targeting to vacuoles for degradation. Further studies focusing on the transport of endosome-specific proteins upon drug treatment will elaborate the mechanism by which vesicle trafficking plays a role in the fungicidal action of fludioxonil. The endocytic pathway is essential for polarized growth and survival in filamentous fungi. In the *C. albicans* model, fludioxonil completely inhibited hyphal growth, whereas the growth of the yeast form of *C. albicans* remained unaffected. Interestingly, deletion of *VPS11*, *VPS16*, and *VPS18* showed synthetic lethality with TOR1 and affected TOR1 signaling (58). Therefore, fludioxonil can inhibit a number of crucial physiological processes through its effect on endosomal trafficking downstream of HHK3 in addition to its effect on the HOG pathway. Interestingly, the vesicle trafficking and secretory pathways have been proposed to be the next-generation target for developing antifungal agents as a few recently discovered fungicides appear to act through these processes (59, 60). Our study further supports this proposition.

The present study has raised an interesting possibility that HHK3 may have a physiological role in endosomal vesicle trafficking in fungi. Deletion of HHK3 had pleiotropic effects. Concomitant to its established role in osmoadaptation, the HHK3 deletion mutants showed an osmosensitive phenotype. Besides this, hyphal growth, virulence, and conidiation were also found to be highly compromised in the deletion mutants in most species (14). Interestingly, vesicle trafficking has a vital role in all these processes. Therefore, it may be possible that HHK3 regulates hyphal growth, virulence, and conidiation by modulating endosomal trafficking through the CORVET complex. Taken together, our study, for the first time, provides novel insight into the function of HHK3 that can be exploited for developing antifungal agents for therapeutic uses.

Experimental procedures

Growth conditions

S. cerevisiae strains were grown in standard conditions at 30 °C in YPD and SD minimal medium with required supplements. *C. albicans* strains were grown at 30 °C in YPD or at 37 °C in Spider medium for inducing hypha formation.

Construction of S. cerevisiae overexpression plasmids

An ~2.3-kb fragment encoding *S. cerevisiae VPS9* gene (along with its promoter and terminator region) was amplified from the genomic DNA and cloned into multicopy plasmid vector pRS426 at the BamHI/XhoI site to obtain pRS426-VPS9. Similarly, pRS426-VPS8, pRS426-VPS11, pRS426-VPS16, pRS426-VPS18, pRS426-VPS34, pRS426-VAM3, pRS426-VAM6, pRS426-VAM7, pRS426-SLT2, pRS426-BCK1, and pRS426-VMA21 were made by cloning the respective PCR fragments. All the clones were confirmed by digestion and sequencing.

Construction of C. albicans strains overexpressing CaVPS16 and CaVPS18

The 2841-bp orf19.6848 corresponding to *CaVPS16* and 2433-bp orf19.5584 corresponding to *CaVPS18* were amplified from SC5314 genomic DNA using primer pairs Vps16XhoIF/Vps16SphIR and VPS18XhoIF/VPS18SphIR, respectively. The PCR products were purified and cloned into pVT50 vector at XhoI/SphI sites to obtain the plasmids pCaVPS16 and pCaVPS18. These plasmids were linearized with StuI and transformed into *C. albicans* strains by electroporation. The transformants were selected on YPD agar containing 200 μg/ml nourseothricin. To confirm the integration of the plasmid, genomic DNA from the transformants was isolated, and diagnostic PCR was carried out using primers pairs ACT1PrF and Vps16SphIR and ACT1PrF and VPS18SphIR. Nucleotide sequencing of the PCR product further confirmed the desired integration. The sequences of primers will be made available upon request.

Western blotting

Levels of dually phosphorylated Hog1p in *S. cerevisiae* strain were detected by Western blotting as described earlier (13). Cells were treated with 5 μg/ml fludioxonil for various time periods ranging from 5 min to 1 h. The total cell extract (~20 μg of protein) from each sample was blotted onto nitrocellulose membrane, and the dually phosphorylated Hog1p was detected using anti-dually phosphorylated p38 antibody (Cell Signaling Technology). The level of Hog1p was detected in the same blot after reprobing with anti-Hog1p antibody (Y-215, Santa Cruz Biotechnology).

Yeast two-hybrid assay

For the two-hybrid assay, pJG4-5 and pEG202 were used as vectors for constructing prey and bait, respectively (61). A ~0.7-kb fragment corresponding to YPD1 ORF (aa 2–167) along with the 3′ region was PCR-amplified using primers Ypd1 2-XhoIF and Ypd1 167-BamHIR and cloned in bait vector pJG4-5 at XhoI and BamHI sites. An ~2.0-kb DNA fragment corresponding to the kinase and receiver domain of Sln1 (aa 566–1220) was PCR-amplified using SLN1-566-BamHIF and SLN1-XhoIR primers and cloned in prey vector pEG202 at BamHI and XhoI restriction sites. Similarly, an ~1.8-kb DNA corresponding to the kinase and receiver domain of ClNik1 (aa 490–1082) was PCR-amplified using ClNik1-490 EcoRIBlunt F and ClNik1-XhoIR primers and cloned in prey vector pEG202 at EcoRI (blunt-ended) and XhoI sites. Authenticity of all the constructs was confirmed by nucleotide sequencing. *S. cerevisiae* strain EGY 48 was cotransformed with bait and prey constructs and selected on minimal medium with 2% glucose and

without tryptophan and histidine. Cotransformed cells were grown to an A_{600} of ~1.0, and 5 μl of the cultures (normalized to an A_{600} of 1.0) was spotted onto minimal medium with 2% galactose and 1% raffinose and without tryptophan, histidine, and leucine. Plates were incubated for 4 days at 30 °C.

Microscopy

S. cerevisiae strain BY4741 harboring plasmids pClNIK1 and pHog1-GFP were grown in SD medium (−His,−Ura) to an A_{600} of 0.5–0.7. An aliquot of the culture was exposed to 0.4 M NaCl for 15 min to serve as a positive control. The remaining portion of the culture was exposed to 5 μg/ml fludioxonil, and the samples were withdrawn at different time points (5, 15, 30, 60, and 180 min). All the samples were immediately fixed with 4% paraformaldehyde. Cells were washed twice with PBS and stained with DAPI before being observed under a Nikon A1R confocal microscope.

S. cerevisiae strain BY4741/pClNIK1 was grown in SD (−His) minimal medium to early log phase (~0.3 A_{600}). After transferring the cultures to fresh medium, the cells were treated with α-factor (6 μg/ml) for 90 min. After washing the cells with ice-cold water to remove α-factor, the cells were suspended in fresh SD (−His) or SD (−His) containing 25 μg/ml fludioxonil. Samples were collected at different time intervals and fixed with 4% paraformaldehyde. Quantification of bud formation and nuclear division during cell cycle progression in these samples was performed by microscopic observation after staining the cells with DAPI. At least 100 cells were counted for each time point.

S. cerevisiae strain BY4741/pClNIK1 was grown at 30 °C to early logarithmic phase in SD medium (−His). The cells were incubated further for 1 h in the presence or absence of 5 μg/ml fludioxonil. Cells were collected by centrifugation, and the cell pellet was resuspended in 50 μl of YPD or YPD containing 5 μg/ml fludioxonil. 1 μl of FM4-64 solution (1.6 μM in DMSO) was added to each aliquot and incubated for 20 min at 30 °C. Cells were centrifuged, and the supernatant was discarded. The cell pellet was resuspended in 5 ml of YPD or YPD containing 5 μg/ml fludioxonil and incubated further for 90 min at 30 °C. Following centrifugation, the cells were resuspended in 50 μl of SD (−His) medium with or without 5 μg/ml fludioxonil and observed under a Nikon A1R confocal microscope.

FRAP experiments were carried as described earlier (53). *C. albicans* strain Sec4-GFP was grown at 37 °C in Spider medium for 45 min to induce hypha formation. Subsequently, fludioxonil (50 μg/ml) was added to the culture and incubated further for 45 min at 37 °C. The cells were then embedded in 0.4% agar on glass slides, maintained at 37 °C by a heated stage, and imaged using a Nikon Eclipse TiE microscope equipped with an Andor iXON3 electron-multiplying charge-coupled device camera and controlled using Andor iQ2.7 software. The protocol was standardized, and a total of 2 min was recorded with prebleaching for 30 s, bleaching at 75% laser power for 30 s, and postbleaching for 60 (control) and 180 s (with fludioxonil). A nonbleached tip in the same field served as a control for bleaching during the image acquisition in the recovery period. Raw values were subjected to subtraction of background. For each time point, the fraction of FRAP was calculated according to the formula $(I_t - I_b)/(I_0 - I_t) \times 100\%$ where t is the time in seconds, I_0 is the intensity prebleaching, I_b is the intensity immediately postbleach, and I_t is the intensity at time t.

Estimation of intracellular glycerol

For determination of intracellular glycerol, *S. cerevisiae* strains harboring pClNIK1 were grown in SD minimal medium up to mid-exponential phase and incubated further for 3 h with or without 25 μg/ml fludioxonil. Cells from 10 ml of culture were collected by centrifugation and washed with chilled medium followed by chilled 0.5 M Tris-HCl (pH 7.5). Finally, the pellet was resuspended in 2 ml of Tris-HCl (pH 7.5). 600 μl of the cell suspension was placed in a microcentrifuge tube and incubated at 100 °C for 10 min. Subsequently, the cells were centrifuged at 5000 rpm for 5 min, and the supernatant was used to estimate glycerol using a UV glycerol assay kit (R-Biopharm) according to the manufacturer's instructions.

Deletion sensitivity profiling

The lithium acetate/single-stranded (LiAc/SS) carrier DNA/PEG method (37) was used to transform the pClNIK1 in the haploid deletion strain collection of *S. cerevisiae* obtained from EUROSCARF. Deletion strains from 96-well plates were patched on 140-mm YPD plates with the help of a 96-well pin tool and grown for 12–16 h. The strains were then transferred by the pin tool to 96-well round bottom microtiter plates containing 50 μl of water in each well. The plates were then centrifuged at 2500 rpm for 10 min, and water was discarded. 50 μl of transformation mixture containing the plasmid pClNIK1 (200 ng) was added to each well. The contents of the plates were mixed on a Thermomixer (Eppendorf) at 800 rpm for 2 min. 100 μl of 50% PEG was then added, and a multichannel pipette was used to mix the contents until the cell suspensions were homogenous. Microtiter plates were then incubated at 42 °C for 1 h on a Thermomixer. After heat shock, the plates were centrifuged at 2500 rpm for 10 min, and the supernatant was discarded. The transformed cell pellets were transferred to SD (−His) plates using a 96-well pin tool. The plates were then incubated at 30 °C for 3–4 days.

The transformants that appeared on the plates were transferred to a 96-well flat bottom microtiter plate containing 100 μl of SD (−His) medium in each well. The plate was incubated at 30 °C for 24 h. 3 μl of the culture from each well of this plate was inoculated into a fresh 96-well plate containing (in each well) 97 μl of SD (−His) medium without or with 0.76 μg/ml fludioxonil. After measuring the initial A_{600} in an ELISA reader, the plates were then incubated at 30 °C. The growth of each strain was recorded using an ELISA reader after 24 h. The strains that showed increased sensitivity compared with the control (BY4741/pClNIK1) were separately picked and archived by making glycerol stocks.

Estimation of DNA content of the cell by FACS

To analyze the DNA content by FACS, *S. cerevisiae* strain BY4742/pClNIK1 was grown in SD minimal medium to ~0.3 A_{600} and exposed to fludioxonil (25 μg/ml) for 4 h. Cells were harvested by centrifugation and fixed in 70% ethanol. Prior to FACS analysis, cells were washed with PBS to remove ethanol

and treated with RNase A at 37 °C for 2 h. Cells were stained with 25 μg/ml propidium iodide, washed, and sonicated briefly to disrupt the cell aggregates before analysis on a BD FACSCalibur for forward scattering. A total of 50,000 events were captured.

Subcellular fractionation

Subcellular fractionation was carried out following the protocol described earlier (44). Briefly, *S. cerevisiae* strain expressing Vps8-GFP and ClNik1p was grown to logarithmic phase (A_{600} ~0.8) in minimal medium and treated with fludioxonil (5 μg/ml) for 4 h. Cells were harvested by centrifugation and resuspended in 0.1 M Tris (pH 9.4) supplemented with 10 mM β-mercaptoethanol and incubated at 30 °C for 10 min. Subsequently, the cells were collected and incubated in buffer (1 M sorbitol, 50 mM Tris-Cl (pH 7.9), and 5 units/μl Zymolyase) to make spheroplasts. Spheroplasts were resuspended in lysis buffer (20 mM HEPES (pH 6.8), 0.2 M Sorbitol, 2 mM EDTA, 50 mM potassium acetate, and protease inhibitor mixture) and homogenized. The lysate was clarified by two rounds of centrifugations at 1000 × *g* for 5 min followed by 13,000 × *g* for 15 min. The supernatant fraction was then centrifuged at 100,000 × *g* for 45 min to obtain the pellet (P100) and supernatant (S100). Equal amounts of protein (100 μg) from each fraction were used for Western blotting using anti-GFP antibody.

LY uptake assay

The LY uptake assay was performed as described previously (45). In brief, BY4741/pClNIK1 cells at logarithmic phase (A_{600} ~0.8) were treated with or without 10 μg/ml fludioxonil for 120 min at 30 °C. Cells were resuspended in YPD (~2–5 A_{600}) and incubated for 45 min at 30 °C in the presence of 4 mg/ml LY (Sigma). The cells were washed three times in 1 ml of ice-cold buffer (50 mM sodium phosphate, 10 mM sodium azide, and 10 mM sodium fluoride (pH 7.5)). Samples were viewed by a Nikon A1R confocal microscope using FITC optics.

FM4-64 recycling assay

The recycling assay was performed as described previously (45). Briefly, *S. cerevisiae* strain BY4741/pClNIK1 was grown to logarithmic phase (A_{600} ~0.8) in minimal medium. The cells were incubated further for 120 min at 30 °C with or without 10 μg/ml fludioxonil. Cells were harvested, resuspended in YPD, and incubated with 40 μM FM4-64 for 10–12 min at 30 °C with shaking. Cells were then diluted in ice-cold SD medium and harvested by centrifugation at low speed. Cells were then washed vigorously three times with ice-cold SD medium and kept on ice. Prior to measuring the fluorescence, prewarmed SD medium was added to the cells to obtain a final A_{600} of 0.25. The fluorescence was recorded for 20 min on a Shimadzu Cary spectrofluorometer with excitation at 515 nm and emission at 680 nm.

Statistical analysis

Statistical analysis was performed using Student's *t* test (two-tailed) and two-way analysis of variance in Microsoft Excel, and *p* values <0.05 were considered significant.

Author contributions—A. R., D. K., and A. S. data curation; A. R., D. K., and A. S. formal analysis; A. R., D. K., and A. S. investigation; A. R., D. K., and A. S. visualization; A. R., D. K., and A. S. methodology; A. R., D. K., A. S., and A. K. M. writing-original draft; A. R., R. P., and A. K. M. writing-review and editing; R. P. and A. K. M. conceptualization; R. P. and A. K. M. funding acquisition; R. P. and A. K. M. project administration; A. K. M. supervision.

Acknowledgments—We thank S. Hohman for yeast strains 507 and 512. Plasmid pVT50 was a kind gift from D. Sanglard, University of Lausanne and University Hospital Center, Lausanne, Switzerland to R. P. C. albicans strains WYZ9 and Sec4-GFP are kind gifts from Y. Wang, National University of Singapore, Singapore and P. E. Sudbery, University of Sheffield, United Kingdom, respectively.

References

1. Brown, G. D., Denning, D. W., Gow, N. A., Levitz, S. M., Netea, M. G., and White, T. C. (2012) Hidden killers: human fungal infections. *Sci. Transl. Med.* **4,** 165rv13 CrossRef Medline
2. Denning, D. W., and Bromley, M. J. (2015) How to bolster the antifungal pipeline. *Science* **347,** 1414–1416 CrossRef Medline
3. Scorzoni, L., de Paula E. Silva, A. C., Marcos, C. M., Assato, P. A., de Melo, W. C., de Oliveira, H. C., Costa-Orlandi, C. B., Mendes-Giannini, M. J., and Fusco-Almeida, A. M. (2017) Antifungal therapy: new advances in the understanding and treatment of mycosis. *Front. Microbiol.* **8,** 36 CrossRef Medline
4. Myung, K., and Klittich, C. J. (2015) Can agricultural fungicides accelerate the discovery of human antifungal drugs? *Drug Discov. Today* **20,** 7–10 CrossRef Medline
5. Corran, A., Knauf-Beiter, G., and Zeun, R. (2008) Fungicides acting on signal transduction, in *Modern Crop Protection Compounds* (Krämer, W., and Schirmer, U., eds) pp. 561–580, Wiley-VCH Verlag GmbH, Weinheim, Germany
6. Tanaka, T., and Izumitsu, K. (2010) Two-component signaling system in filamentous fungi and the mode of action of dicarboximide and phenylpyrrole fungicides, in *Fungicides* (Carisse, O., ed), pp. 523–538, InTech, London
7. Kilani, J., and Fillinger, S. (2016) Phenylpyrroles: 30 years, two molecules and (nearly) no resistance. *Front. Microbiol.* **7,** 2014 CrossRef Medline
8. Hohmann, S. (2002) Osmotic stress signaling and osmoadaptation in yeasts. *Microbiol. Mol. Biol. Rev.* **66,** 300–372 CrossRef Medline
9. Zhang, Y., Lamm, R., Pillonel, C., Lam, S., and Xu, J. R. (2002) Osmoregulation and fungicide resistance: the *Neurospora crassa os-2* gene encodes a *HOG1* mitogen-activated protein kinase homologue. *Appl. Environ. Microbiol.* **68,** 532–538 CrossRef Medline
10. Hagiwara, D., Asano, Y., Marui, J., Yoshimi, A., Mizuno, T., and Abe, K. (2009) Transcriptional profiling for *Aspergillus nidulans* HogA MAPK signaling pathway in response to fludioxonil and osmotic stress. *Fungal Genet. Biol.* **46,** 868–878 CrossRef Medline
11. Kojima, K., Bahn, Y. S., and Heitman, J. (2006) Calcineurin, Mpk1 and Hog1 MAPK pathways independently control fludioxonil antifungal sensitivity in *Cryptococcus neoformans. Microbiology* **152,** 591–604 CrossRef Medline
12. Cui, W., Beever, R. E., Parkes, S. L., Weeds, P. L., and Templeton, M. D. (2002) An osmosensing histidine kinase mediates dicarboximide fungicide resistance in *Botryotinia fuckeliana* (*Botrytis cinerea*). *Fungal Genet. Biol.* **36,** 187–198 CrossRef Medline
13. Meena, N., Kaur, H., and Mondal, A. K. (2010) Interactions among HAMP repeats act as an osmosensing molecular switch in a group III hybrid histidine kinase. *J. Biol. Chem.* **285,** 12121–12132 CrossRef Medline
14. Defosse, T. A., Sharma, A., Mondal, A. K., Dugé de Bernonville, T., Latgé, J. P., Calderone, R., Giglioli-Guivarc'h, N., Courdavault, V., Clastre, M., and Papon, N. (2015) Hybrid histidine kinases in pathogenic fungi. *Mol. Microbiol.* **95,** 914–924 CrossRef Medline

15. Ochiai, N., Fujimura, M., Motoyama, T., Ichiishi, A., Usami, R., Horikoshi, K., and Yamaguchi, I. (2001) Characterization of mutations in the two-component histidine kinase gene that confer fludioxonil resistance and osmotic sensitivity in the *os-1* mutants of *Neurospora crassa*. *Pest Manag. Sci.* **57,** 437–442 CrossRef Medline
16. Yoshimi, A., Kojima, K., Takano, Y., and Tanaka, C. (2005) Group III histidine kinase is a positive regulator of Hog1-type mitogen-activated protein kinase in filamentous fungi. *Eukaryot. Cell* **4,** 1820–1828 CrossRef Medline
17. Avenot, H., Simoneau, P., Iacomi-Vasilescu, B., and Bataillé-Simoneau, N. (2005) Characterization of mutations in the two-component histidine kinase gene *AbNIK1* from *Alternaria brassicicola* that confer high dicarboximide and phenylpyrrole resistance. *Curr. Genet.* **47,** 234–243 CrossRef Medline
18. Oshima, M., Banno, S., Okada, K., Takeuchi, T., Kimura, M., Ichiishi, A., Yamaguchi, I., and Fuzimura, M. (2006) Survey of mutations of a histidine kinase gene BcOS1 in dicarboximide-resistant field isolates of *Botrytis cinerea*. *J. Gen. Plant Pathol.* **72,** 65–73 CrossRef
19. Motoyama, T., Ohira, T., Kadokura, K., Ichiishi, A., Fujimura, M., Yamaguchi, I., and Kudo, T. (2005) An Os-1 family histidine kinase from a filamentous fungus confers fungicide-sensitivity to yeast. *Curr. Genet.* **47,** 298–306 CrossRef Medline
20. Furukawa, K., Randhawa, A., Kaur, H., Mondal, A. K., and Hohmann, S. (2012) Fungal fludioxonil sensitivity is diminished by a constitutively active form of the group III histidine kinase. *FEBS Lett.* **586,** 2417–2422 CrossRef Medline
21. Randhawa, A., and Mondal, A. K. (2013) The sixth HAMP domain negatively regulates the activity of the group III HHK containing seven HAMP domains. *Biochem. Biophys. Res. Commun.* **438,** 140–144 CrossRef Medline
22. Kaur, H., Singh, S., Rathore, Y. S., Sharma, A., Furukawa, K., Hohmann, S., Ashish, and Mondal, A. K. (2014) Differential role of HAMP-like linkers in regulating the functionality of the group III histidine kinase DhNik1p. *J. Biol. Chem.* **289,** 20245–20258 CrossRef Medline
23. Alex, L. A., Borkovich, K. A., and Simon, M. I. (1996) Hyphal development in *Neurospora crassa*, involvement of a two-component histidine kinase. *Proc. Natl. Acad. Sci. U.S.A.* **93,** 3416–3421 CrossRef Medline
24. Chapeland-Leclerc, F., Paccallet, P., Ruprich-Robert, G., Reboutier, D., Chastin, C., and Papon, N. (2007) Differential involvement of histidine kinase receptors in pseudohyphal development, stress adaptation, and drug sensitivity of the opportunistic yeast *Candida lusitaniae*. *Eukaryot. Cell* **6,** 1782–1794 CrossRef Medline
25. Bahn, Y. S., Kojima, K., Cox, G. M., and Heitman, J. (2006) A unique fungal two-component system regulates stress responses, drug sensitivity, sexual development, and virulence of *Cryptococcus neoformans*. *Mol. Biol. Cell* **17,** 3122–3135 CrossRef Medline
26. Rispail, N., and Di Pietro, A. (2010) The two-component histidine kinase Fhk1 controls stress adaptation and virulence of *Fusarium oxysporum*. *Mol. Plant Pathol.* **11,** 395–407 CrossRef Medline
27. Duan, Y., Ge, C., Liu, S., Wang, J., and Zhou, M. (2013) A two-component histidine kinase Shk1 controls stress response, sclerotial formation and fungicide resistance in *Sclerotinia sclerotiorum*. *Mol. Plant Pathol.* **14,** 708–718 CrossRef Medline
28. Hagiwara, D., Takahashi-Nakaguchi, A., Toyotome, T., Yoshimi, A., Abe, K., Kamei, K., Gonoi, T., and Kawamoto, S. (2013) NikA/TcsC histidine kinase is involved in conidiation, hyphal morphology, and responses to osmotic stress and antifungal chemicals in *Aspergillus fumigatus*. *PLoS One* **8,** e80881 CrossRef Medline
29. Spang, A. (2016) Membrane tethering complexes in the endosomal system. *Front. Cell Dev. Biol.* **4,** 35 CrossRef Medline
30. Randhawa, A., Chawla, S., and Mondal, A. K. (2016) Functional dissection of HAMP domains in *NIK1* ortholog from pathogenic yeast *Candida lusitaniae*. *Gene* **577,** 251–257 CrossRef Medline
31. Nevoigt, E., and Stahl, U. (1997) Osmoregulation and glycerol metabolism in the yeast *Saccharomyces cerevisiae*. *FEMS Microbiol. Rev.* **21,** 231–241 CrossRef Medline
32. Ferrigno, P., Posas, F., Koepp, D., Saito, H., and Silver, P. A. (1998) Regulated nucleo/cytoplasmic exchange of *HOG1* MAPK requires the importin beta homologs *NMD5* and *XPO1*. *EMBO J.* **17,** 5606–5614 CrossRef Medline
33. Ericson, E., Hoon, S., St Onge, R. P., Giaever, G., and Nislow, C. (2010) Exploring gene function and drug action using chemogenomic dosage assays. *Methods Enzymol.* **470,** 233–255 CrossRef Medline
34. Roemer, T., Davies, J., Giaever, G., and Nislow, C. (2011) Bugs, drugs and chemical genomics. *Nat. Chem. Biol.* **8,** 46–56 CrossRef Medline
35. Gietz, R. D., and Schiestl, R. H. (2007) Microtiter plate transformation using LiAc/SS carrier DNA/PEG method. *Nat. Protoc.* **2,** 5–8 CrossRef Medline
36. Parsons, A. B., Lopez, A., Givoni, I. E., Williams, D. E., Gray, C. A., Porter, J., Chua, G., Sopko, R., Brost, R. L., Ho, C. H., Wang, J., Ketela, T., Brenner, C., Brill, J. A., Fernandez, G. E., *et al.* (2006) Exploring the mode-of-action of bioactive compounds by chemical-genetic profiling in yeast. *Cell* **126,** 611–625 CrossRef Medline
37. Levin, D. E. (2011) Regulation of cell wall biogenesis in *Saccharomyces cerevisiae*: the cell wall integrity signaling pathway. *Genetics.* **189,** 1145–1175 CrossRef Medline
38. Vallen, E. A., Caviston, J., and Bi, E. (2000) Roles of Hof1p, Bni1p, Bnr1p, and Myo1p in cytokinesis in *Saccharomyces cerevisiae*. *Mol. Biol. Cell* **11,** 593–611 CrossRef Medline
39. Graziano, B. R., Yu, H. Y., Alioto, S. L., Eskin, J. A., Ydenberg, C. A., Waterman, D. P., Garabedian, M., and Goode, B. L. (2014) The F-BAR protein Hof1 tunes formin activity to sculpt actin cables during polarized growth. *Mol. Biol. Cell* **25,** 1730–1743 CrossRef Medline
40. Wickner, W. (2010) Membrane fusion: five lipids, four SNAREs, three chaperones, two nucleotides, and a Rab, all dancing in a ring on yeast vacuoles. *Annu. Rev. Cell Dev. Biol.* **26,** 115–136 CrossRef Medline
41. Cain, C. W., Lohse, M. B., Homann, O. R., Sil, A., and Johnson, A. D. (2012) A conserved transcriptional regulator governs fungal morphology in widely diverged species. *Genetics* **190,** 511–521 CrossRef Medline
42. Huang, D. W., Sherman, B. T., and Lempicki, R. A. (2009) Systematic and integrative analysis of large gene lists using DAVID bioinformatics resources. *Nat. Protoc.* **4,** 44–57 CrossRef Medline
43. Mostafavi, S., Ray, D., Warde-Farley, D., Grouios, C., and Morris, Q. (2008) GeneMANIA: a real-time multiple association network integration algorithm for predicting gene function. *Genome Biol.* **9,** S4 CrossRef Medline
44. Epp, N., and Ungermann, C. (2013) The N-terminal domains of Vps3 and Vps8 are critical for localization and function of the CORVET tethering complex on endosomes. *PLoS One* **8,** e67307 CrossRef Medline
45. Wiederkehr, A., Avaro, S., Prescianotto-Baschong, C., Haguenauer-Tsapis, R., and Riezman, H. (2000) The F-box protein Rcy1p is involved in endocytic membrane traffic and recycling out of an early endosome in *Saccharomyces cerevisiae*. *J. Cell Biol.* **149,** 397–410 CrossRef Medline
46. Riquelme, M. (2013) Tip growth in filamentous fungi: a road trip to the apex. *Annu. Rev. Microbiol.* **67,** 587–609 CrossRef Medline
47. Veses, V., Richards, A., and Gow, N. A. (2008) Vacuoles and fungal biology. *Curr. Opin. Microbiol.* **11,** 503–510 CrossRef Medline
48. Steinberg, G. (2014) Endocytosis and early endosome motility in filamentous fungi. *Curr. Opin. Microbiol.* **20,** 10–18 CrossRef Medline
49. Palmer, G. E., Cashmore, A., and Sturtevant, J. (2003) *Candida albicans* VPS11 is required for vacuole biogenesis and germ tube formation. *Eukaryot. Cell* **2,** 411–421 Medline
50. Braun, B. R., and Johnson, A. D. (1997) Control of filament formation in *Candida albicans* by the transcriptional repressor *TUP1*. *Science* **277,** 105–109 CrossRef Medline
51. Zheng, X. D., Wang, Y. M., and Wang, Y. (2003) *CaSPA2* is important for polarity establishment and maintenance in *Candida albicans*. *Mol. Microbiol.* **49,** 1391–1405 CrossRef Medline
52. Jones, L. A., and Sudbery, P. E. (2010) Spitzenkorper, exocyst, and polarisome components in *Candida albicans* hyphae show different patterns of localization and have distinct dynamic properties. *Eukaryot. Cell* **9,** 1455–1465 CrossRef Medline
53. Lawry, S. M., Tebbets, B., Kean, I., Stewart, D., Hetelle, J., and Klein, B. S. (2017) Fludioxonil induces Drk1, a fungal group III hybrid histidine kinase, to dephosphorylate its downstream target, Ypd1. *Antimicrob. Agents Chemother.* **61,** e01414–16 CrossRef Medline

54. Zhu, Y., Qin, L., Yoshida, T., and Inouye, M. (2000) Phosphatase activity of histidine kinase EnvZ without kinase catalytic domain. *Proc. Natl. Acad. Sci. U.S.A.* **97,** 7808–7813 CrossRef Medline
55. Catlett, N. L., Yoder, O. C., and Turgeon, B. G. (2003) Whole-genome analysis of two-component signal transduction genes in fungal pathogens. *Eukaryot. Cell* **2,** 1151–1161 CrossRef Medline
56. Neto, H., Collins, L. L., and Gould, G. W. (2011) Vesicle trafficking and membrane remodelling in cytokinesis. *Biochem. J.* **437,** 13–24 CrossRef Medline
57. Solinger, J. A., and Spang, A. (2013) Tethering complexes in the endocytic pathway: CORVET and HOPS. *FEBS J.* **280,** 2743–2757 CrossRef Medline
58. Zurita-Martinez, S. A., Puria, R., Pan, X., Boeke, J. D., and Cardenas, M. E. (2007) Efficient Tor signaling requires a functional class C Vps protein complex in *Saccharomyces cerevisiae*. *Genetics* **176,** 2139–2150 CrossRef Medline
59. Djordjevic, J. T., and Lev, S. (2018) Fungal secretion: the next-gen target of antifungal agents? *Cell Chem. Biol.* **25,** 233–235 CrossRef Medline
60. Alspaugh, J. A. (2016) Discovery of ibomycin, a potent antifungal weapon. *Cell Chem. Biol.* **23,** 1321–1322 CrossRef Medline
61. Golemis, E. A., and Brent, R. (1997) Searching for interacting proteins with the two hybrid system III, in The Yeast Two Hybrid System (Bartel, P. L., and Fields, S., eds) pp 43–72, Oxford University Press, Oxford, UK